Multi-scale three-dimensional variational data assimilation for high-resolution aerosol observations: Methodology and application

Zengliang ZANG[1], Yanfei LIANG[1,2*], Wei YOU[1†], Yi LI[1], Xiaobin PAN[1] & Zhijin LI[3,4]

[1] *College of Meteorology and Oceanography, National University of Defense Technology, Changsha 410073, China;*
[2] *No.32145 Unit of PLA, Xinxiang 453000, China;*
[3] *Department of Atmospheric and Oceanic Sciences, Fudan University, Shanghai 200433, China;*
[4] *Joint Institute for Regional Earth System Science and Engineering, University of California Los Angeles, California 91109, USA*

Abstract   With an increasing number of air quality monitoring stations installed around the Chinese mainland, high-resolution aerosol observations become available, allowing improvements in air pollution monitoring and aerosol forecasting. However, the multi scales (especially small-scale) information included in high-resolution aerosol observations could not be effectively utilized by the traditional three-dimensional variational method (3DVAR). This study attempted to extend the traditional 3DVAR to a multi-scale 3DVAR with two iteration steps, two-scale-3DVAR (TS-3DVAR), to improve the effectiveness of assimilating high-resolution observations. In TS-3DVAR, the large-scale and small-scale components of observation information were decomposed from the original high-resolution observations using a Gaussian smoothing method and then assimilated using the corresponding large-scale or small-scale background error covariances which were derived from the partitioned background error samples. The data assimilation (DA) analysis field generated by TS-3DVAR is more accurate than 3DVAR in reproducing the field's multi-scale characteristics, which could thus be used as the initial chemical field of the air quality model to improve aerosol forecasting. Particulate matter with an aerodynamic diameter of less than 2.5 μm ($PM_{2.5}$) and 10.0 μm (PM_{10}) from the surface air quality monitoring stations from November 01 to November 30, 2018 at 00:00 were assimilated daily to verify the effects of TS-3DVAR and 3DVAR on the aerosol analysis and forecast accuracy. The results showed that TS-3DVAR better constrained both large-scale and small-scale, especially the spatial wavelengths in a range of 54–216 km and those above 351 km. The average power spectra of the TS-3DVAR assimilation increment in the two wavelength ranges were 71.70% and 35.33% higher than those of 3DVAR. As a result, the TS-3DVAR was more effective than 3DVAR in improving the accuracy of the initial chemical field, and thereby the forecasting capability for $PM_{2.5}$. In the initial chemical field, the 30-day average correlation coefficient (Corr) of $PM_{2.5}$ of TS-3DVAR was 0.052 (6.12%) higher than that of 3DVAR, and the root mean square error (RMSE) of TS-3DVAR was 3.446 μg m^{-3} (16.4%) lower than that of 3DVAR. For the forecasting capability for $PM_{2.5}$ mass concentration, the 30-day average Corr of TS-3DVAR during the 0–24 hour forecast period was 0.025 (5.08%) higher than that of 3DVAR, and the average RMSE was 2.027 μg m^{-3} (4.85%) lower. The positive effect of TS-3DVAR on the improvement of forecasting capability can last for more than 24 h.

Keywords   Multi-scale, 3DVAR, Data assimilation, Aerosol forecast, WRF-Chem

* Corresponding author (email: 13270805867@163.com)
† Corresponding author (email: ywlx_1987@163.com)

1. Introduction

An air pollution monitoring network, with over 2000 monitoring stations, has been established across the Chinese mainland to provide observations for controlling air pollution and improving air quality forecast (Sun et al., 2020). High-resolution aerosol observations collected by the network have been used for systematic air quality assessments and air quality model (AQM) development. It has been demonstrated that a three-dimensional variational (3DVAR) data assimilation (DA) method allows sufficiently utilizing observations to improve the accuracy of the initial chemical field and the aerosol emissions for AQM (Benedetti et al., 2009; Tang et al., 2016; Peng et al., 2017; Chen et al., 2019; Feng et al., 2020; Hu et al., 2022), which consequently improve AQM forecast and in turn, enables appropriate management of air pollution to ensure safe air quality levels (Bai et al., 2008; Niu et al., 2008; Sandu and Chai, 2011; Pagowski and Grell, 2012; Jiang et al., 2013; Dai et al., 2014; Bocquet et al., 2015; Yin et al., 2016; Zhu et al., 2018; Xia et al., 2019). However, the traditional 3DVAR is not effective in assimilating multi-scale observations information, especially small-scale components, with high-resolution measurements, which is the major difficulty addressed in this study.

The background error covariance matrix (BEC or **B** matrix) is an important parameter in 3DVAR. It determines the shape and magnitude of DA increments (Ide et al., 1997; Bannister, 2008a, 2008b; Ha and Lee, 2012; Chen et al., 2016; Bannister, 2017; Pang and Wang, 2021). In advanced AQMs, the **B** matrix is too high-dimensional to directly calculate in DA. A simplification is necessary. In general, several other statistical measures, such as the background error standard deviation (BESD), background error vertical correlation coefficients (BEVCC), and horizontal correlation length scale (L), are required to compute (Cheng et al., 2019; Wang et al., 2022). The length scale L is single and set to a fixed value in a traditional 3DVAR method. A given L determines the DA to assimilate observational information on certain scales associated, causing loss of multi-scale information—particularly small-scale information (Xie et al., 2011; Li et al., 2015, 2016). Therefore, there is high potential in DA using high-resolution observational to improve the accuracy of DA analysis and capability of AQM prediction, which has not been fully exploited to date.

Meteorological and oceanographic DA studies have examined the limit when a single L is used. Xie et al. (2011) have indicated that 3DVAR essentially corresponds to a single correction of the Barnes analysis, and that a single Barnes iteration does not yield a good objective analysis. A single correlation length scale 3DVAR may not yield a good analysis if the covariance is unknown or contains incomplete or partial information. Additionally, Li et al. (2015, 2016)

argued that the traditional 3DVAR method is inherently ineffective for fine-resolution models due to its filtering properties; therefore, a multi-scale 3DVAR method was suggested instead. According to Zhang et al. (2014), the BECs corresponding to models with different resolutions have different scales of structure and properties; therefore, it is necessary to develop a multi-scale approach to DA methods to assimilate observations that contain information on different scales. In the context of the utilization rate of observational data, L plays the role of spreading out observational information to nearby grid-points, wherein the larger the L, the larger the spread range which observational information extends in the DA analysis. In general, this means that a larger L is necessary to assimilate more large-scale observational information. However, a larger L also causes the DA to have a stronger filtering effect (Li et al., 2016), by virtue of which it cannot fully utilize small-scale information; hence, giving rise to a notable conflict between the utilization rate of the large-scale and small-scale observational information.

To address the above conflict, researchers in the field of meteorological and oceanographic DA have explored multi-scale DA methodologies. Xie et al. (2011) established a sequential space and time multi-scale analysis system (STMAS) for meteorological data assimilation, wherein observational information on a specific scale was assimilated in each of the multiple iteration steps, indicating that the STMAS could generate an analysis field with multi-scale characteristics. Zhang et al. (2014, 2015) applied a DA scheme that used BEC with multi-scale characteristics to assimilate meteorological data. In the DA analysis increment, there is not only the large-scale information from background fields but also the local information from observations. Thus, the forecast of precipitation with the multi-scale increment is improved. Peng et al. (2010) and Wang et al. (2016) used the scale-selective data assimilation (SSDA) method to adjust the model variables on large scales while keeping them consistent on small scales to preserve the large-scale observational information and the original small-scale information in the model. Li et al. (2015, 2016) developed a multi-scale three-dimensional variational (MS-3DVAR) DA scheme, particularly for high-resolution ocean data assimilation. This resulted in the decomposition of the observational data into different scales, as well as its individual assimilation that depended on the BEC of the corresponding scale. A set of one-dimensional DA experiments to assimilate simulated and actual ocean observations were conducted by Li et al. (2015), Muscarella et al. (2014), Miyazawa et al. (2017) to illustrate how MS-3DVAR improves the effectiveness of the assimilation. The results showed that MS-3DVAR had reduced analysis errors compared with a traditional 3DVAR scheme.

Although significant progress in multi-scale DA methods

has been made in the fields of meteorological and oceano-graphic DA, its application in aerosol data assimilation is still not explored. The aerosol distribution is inherently multi-spatial and small-scale by nature (Xu et al., 2005) due to complex factors such as multi-scale weather systems (Zhang, 2005; Zhu et al., 2013; Liu et al., 2015; Huang et al., 2017), localized emission sources, and small-scale photo-chemical processes (Chen P L et al., 2017; Chen S Y et al., 2017, Han and Zhang, 2021). On the other hand, the hor-izontal spatial resolution of the monitoring network has reached up to 10 km in a number of cities and surrounding areas in eastern China and thus could provide observational information on multi scales. So in-depth studies on the use of the multi-scale DA method are necessary to capitalize the high-resolution aerosol observations and ultimately improve the aerosol forecasting capabilities.

Hence, this study aims to develop a multi-scale 3DVAR method with two iteration steps, two-scale-3DVAR (TS-3DVAR), based on the traditional 3DVAR system by Li et al. (2013), Zang et al. (2016), Wang et al. (2020), and Liang et al. (2020). This study also leveraged the AQM of WRF-Chem [Weather Research and Forecasting (WRF) model coupled with online chemistry]. The actual $PM_{2.5}$ and PM_{10} mass concentrations measurements across the Chinese mainland were assimilated to illustrate the advantages of the TS-3DVAR over 3DVAR.

2. Materials and methods

2.1 AQM and data source

This study used the WRF-Chem model version 3.9.1 as the AQM, wherein the simulation region contained 164×155 grid points with a spacing of 27 km, and the center of the region was located at 109.4°E, 36°N (Figure 1). The physical and chemical schemes that were used followed that of Liang et al. (2020), while the aerosol scheme was the Model for Simulating Aerosol Interactions and Chemistry (MOSAIC) with 4 bins (MOSAIC_4bins; Zaveri et al., 2008). With the MOSAIC_4bins, the atmospheric aerosols were divided into 8 components: black/elemental carbon (EC/BC), organic carbon (OC), sulfate (SO4), nitrate (NO3), ammonium salt (NH4), chloride (Cl), sodium salt (Na), and other un-classified inorganic compounds (OIN). Further, the aerosol size was classified into 4 classifications (4bin), namely: 0.0390625–0.15625, 0.15625–0.625, 0.625–2.5, and 2.5–10 μm. Thus, the various aerosols with various sizes were represented by 32 model variables.

The mass concentration (MC) measurements of $PM_{2.5}$ and PM_{10} (PMs) were obtained from 1579 air quality monitoring stations. To ensure the temporal and spatial representative-ness of PM data adopted in DA, a quality control process similar to that employed by Liang et al. (2020) was followed,

wherein data thinning was performed in accordance with the model resolution. Specifically, when multiple PM measure-ments are in one grid cell, all data deviating from the mean values of the PM by more than two times the standard de-viation were removed. Thereafter, arithmetic mean values were obtained and considered for both DA and validation (Sun et al., 2020). Among the 720 observation times in November 2018, there were 706 times (98.06%) when the data volume was between 600 and 624, while there were only 14 times (1.94%) when there were no valid observation data.

2.2 The MS-3DVAR algorithm

The MS-3DVAR scheme that was applied in this study in-cludes two scales: large-scale and small-scale, and is referred to as TS-3DVAR. The incremental form of the cost function for the traditional 3DVAR is as follows (Liu et al., 2011; Li et al., 2013):

$$\mathbf{J}(\delta\mathbf{x}) = \frac{1}{2}\delta\mathbf{x}^{\mathrm{T}}\mathbf{B}^{-1}\delta\mathbf{x}$$
$$+ \frac{1}{2}(\mathbf{H}\delta\mathbf{x} - \mathbf{d})^{\mathrm{T}}\mathbf{R}^{-1}(\mathbf{H}\delta\mathbf{x} - \mathbf{d}), \tag{1}$$

here, the $\delta\mathbf{x}$ represents the incremental analysis variable, which is an n-vector defined as $\delta\mathbf{x}=\mathbf{x}-\mathbf{x}^b$, where $\mathbf{x}$ represents the analysis variable; and $\mathbf{x}^b$ is the background variable ob-tained from the model forecast. $\mathbf{B}$ represents the BEC (error covariance associated with $\mathbf{x}^b$) and is an $n\times n$ matrix. The $\mathbf{d}=\mathbf{y}-\mathbf{H}\mathbf{x}^b$ represents the observation innovation and is an m-vector, $\mathbf{y}$ is the observation vector and the $m\times n$ matrix $\mathbf{H}$ is the observational operator that maps the model state variable to the observation. $\mathbf{R}$ represents the observational error covariance and is an $m\times m$-matrix.

Without partitioning the cost function and its parameters into two scales, the TS-3DVAR algorithm is essentially si-milar to the basic 3DVAR algorithm. The cost functions of the TS-3DVAR are as follows:

$$\mathbf{J}(\delta\mathbf{x}_{\mathrm{L}}) = \frac{1}{2}\delta\mathbf{x}_{\mathrm{L}}^{\mathrm{T}}\mathbf{B}_{\mathrm{L}}^{-1}\delta\mathbf{x}_{\mathrm{L}}$$
$$+ \frac{1}{2}(\mathbf{H}\delta\mathbf{x}_{\mathrm{L}} - \mathbf{d}_{\mathrm{L}})^{\mathrm{T}}\mathbf{R}_{\mathrm{L}}^{-1}(\mathbf{H}\delta\mathbf{x}_{\mathrm{L}} - \mathbf{d}_{\mathrm{L}}), \tag{2}$$

$$\mathbf{J}(\delta\mathbf{x}_{\mathrm{S}}) = \frac{1}{2}\delta\mathbf{x}_{\mathrm{S}}^{\mathrm{T}}\mathbf{B}_{\mathrm{S}}^{-1}\delta\mathbf{x}_{\mathrm{S}}$$
$$+ \frac{1}{2}(\mathbf{H}\delta\mathbf{x}_{\mathrm{S}} - \mathbf{d}_{\mathrm{S}})^{\mathrm{T}}\mathbf{R}_{\mathrm{S}}^{-1}(\mathbf{H}\delta\mathbf{x}_{\mathrm{S}} - \mathbf{d}_{\mathrm{S}}), \tag{3}$$

here, all variables are equivalent to the 3DVAR algorithm except for the L and S subscripts which represent the para-meters on the large-scale and small-scale. Both are also partitioned from their original parameters, which is further discussed in Section 2.3. The TS-3DVAR involves a two-step sequential iteration wherein the large-scale observa-tional innovation $\mathbf{d}_{\mathrm{L}}$ is first assimilated to obtain the large-scale incremental field $\delta\mathbf{x}_{\mathrm{L}}$. This is followed by the assim-ilation of the small-scale observation innovation $\mathbf{d}_{\mathrm{S}}$, to obtain

the small-scale incremental field $\boldsymbol{\delta x}_S$. As these steps correspond to the scale of parameters ($\mathbf{B}_L$, $\mathbf{d}_L$ or $\mathbf{B}_S$ and $\mathbf{d}_S$), the final DA analysis field is given by $\mathbf{x}^a = \mathbf{x}^b + \boldsymbol{\delta x}_L + \boldsymbol{\delta x}_S$. To reduce the total number of state variables, Liang et al. (2020) suggested designing two state variables for each aerosol component. Specifically, one state variable corresponds to fine particles and the other to coarse particles. In this study, the former was obtained from the combination of the first three particle-size bins while the latter from the fourth particle-size bin. As a result, a total of 16 state variables in the DA scheme denoted as $EC_{2.5}$, $EC_{2.5-10}$, $OC_{2.5}$, $OC_{2.5-10}$, $SO4_{2.5}$, $SO4_{2.5-10}$, $NO3_{2.5}$, $NO3_{2.5-10}$, $NH4_{2.5}$, $NH4_{2.5-10}$, $CL_{2.5}$, $CL_{2.5-10}$, $NA_{2.5}$, $NA_{2.5-10}$, $OIN_{2.5}$, and $OIN_{2.5-10}$, were obtained.

2.3 Scale decomposition method and B estimation

To implement TS-3DVAR, the observation innovation and the BEC must be partitioned into two different spatial scales. This study used a Gaussian smoothing method for spatial decomposition (Li et al., 2015). Firstly, the observation data is positioned. Thereafter, all data values in the concentrated smooth region were averaged with the weight function in eq. (4). Considerably, this weighted average was used as the large-scale data value at this particular position. Small-scale data values are then obtained by subtracting the large-scale data value from the original data value. The weighted weight function is expressed as follows:

$$w = w_0 e^{-r^2/2D^2}, \tag{4}$$

here, w_0 is a normalization factor; e is the base of the natural logarithm; r is the distance between the data and its neighbors; and D is the Gaussian smoothing length scale.

To distinguish the traditional 3DVAR parameters from the large-scale or small-scale parameters in the TS-3DVAR, the former was referred to as the single-scale parameters. The single-scale observation innovation $\mathbf{d}$ was calculated from the original background field and observations for DA. The $\mathbf{d}$ is partitioned into $\mathbf{d}_L$ and $\mathbf{d}_S$ using the scale decomposition method. The single-scale $\mathbf{B}$ was estimated from the single-scale background error samples, whereas the $\mathbf{B}_L$ and $\mathbf{B}_S$ were estimated from the large-scale and small-scale background error samples, which were obtained from the single-scale background error samples using the scale decomposition method.

The differences between the 24- and 48-h WRF-Chem forecasts during the same November 2018 period were considered as the single-scale background error samples to allow the estimation of $\mathbf{B}$ using the National Meteorological Center (NMC) method (Parrish and Derber, 1992; Cao et al., 2008; Li et al., 2013). The BESD, BEVCC, and L were calculated for each of the 16 state variables (Li et al., 2013; Zang et al., 2015) and its corresponding large-scale and small-scale parameters (BESD$_L$, BESD$_S$, BEVCC$_L$, BEVCC$_S$, L_L and L_S) were also calculated using the scale

Figure 1 The experimental domain (light blue rectangular) and the locations of 1579 ground air quality monitoring stations (red dots).

decomposition method.

2.4 DA and forecast experimental design and verification analysis method

One experiment for each of the 3DVAR (3DVAR) and TS-3DVAR (TS_3DVAR) methods was designed from 0000 UTC 01 November 2018 to 0000 UTC 01 December 2018 to examine the differences between the two methods. A control experiment without observation assimilation (Control) was also used to examine the effects of DA. In both the DA experiments, the 24-h forecast was used as the background field for DA and the PM observations were assimilated at 0000 each day, then the obtained DA analysis field was used as the initial chemical field and the forecasts were performed for another 24 h period. To implement the scale partitioning as described in Section 2.3, the Gaussian smoothing length D was selected as 60 km, or roughly equal to the average single-scale L of all state variables.

The results of the experiments were evaluated using the root mean square error (RMSE) and the correlation coefficients (Corr) that were calculated based on Liang et al. (2020).

$$\text{RMSE} = \sqrt{\frac{1}{N}\sum_{i=1}^{N}(M_i - O_i)^2}, \tag{5}$$

$$\text{Corr} = \frac{\sum_{i=1}^{N}(M_i - \overline{M})(O_i - \overline{O})}{\sqrt{\sum_{i=1}^{N}(M_i - \overline{M})^2 \sum_{i=1}^{N}(O_i - \overline{O})^2}}, \tag{6}$$

$$\overline{M} = \frac{1}{N}\sum_{i=1}^{N}M_i, \tag{7}$$

$$\overline{O} = \frac{1}{N}\sum_{i=1}^{N}O_i, \tag{8}$$

where M_i is the simulated sample; O_i is the measured sample;

N is the number of samples; $\overline{M}$ is the average simulated PM$_{2.5}$; and $\overline{O}$ is the average of the measurements. Here, better performances were reflected by smaller RMSE values and larger Corr values (Boylan and Russell, 2006).

3   Results

3.1   The B matrix on different scales

Table 1 shows the L of the 16 state variables on the single-scale (L), large-scale (L_L), and small-scale (L_S). The average L of all these variables was 60.72 km, which was 2.25 times the grid spacing of 27 km. In contrast, the mean L_L was 107.30 km or 3.97 times the grid spacing, and 76.71% larger than L, whereas the mean L_S was 20.72 km or 0.77 times of the grid spacing, and 65.88% smaller than the L. This finding was attributed to the Gaussian smoothing, which had caused an increase in the horizontal correlation of the background error samples to make the L_L greater than L. Further, since the small-scale background error samples were obtained from the difference of the large-scale and single-scale background error samples, where the former was dominantly greater, the resulting L_S was always smaller than L. Notably, a larger L_L helps spread the large-scale observational information and a smaller L_S helps assimilate more small-scale component in the TS-3DVAR which can result in a more accurate DA analyses compared to 3DVAR.
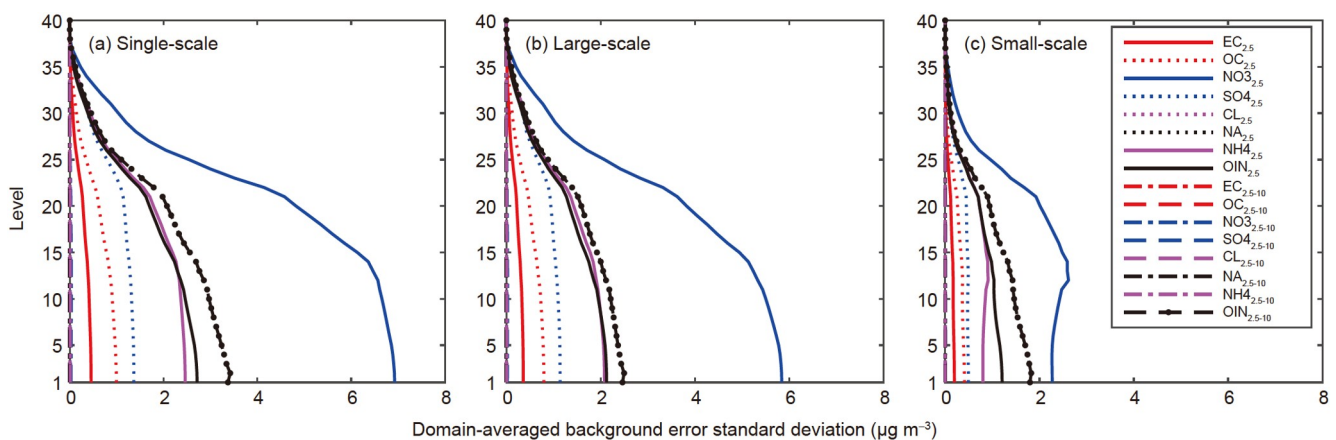
Meanwhile, the domain-averaged BESD vertical profiles for the 16 state variables on the single-scale (BESD), large-scale (BESD$_L$), and small-scale (BESD$_S$) are presented in Figure 2. Here, the BESD was larger than BESD$_L$, which is in contrast to the relative order of magnitude of L, because the original BESD had been reduced due to the Gaussian smoothing. Nevertheless, the relative order of magnitude of the different state variables was similar for all three scales. Seven state variables (NO3$_{2.5}$, OIN$_{2.5-10}$, OIN$_{2.5}$, NH4$_{2.5}$, SO4$_{2.5}$, OC$_{2.5}$ and EC$_{2.5}$) were observed to have the largest near-surface values for all three scales.
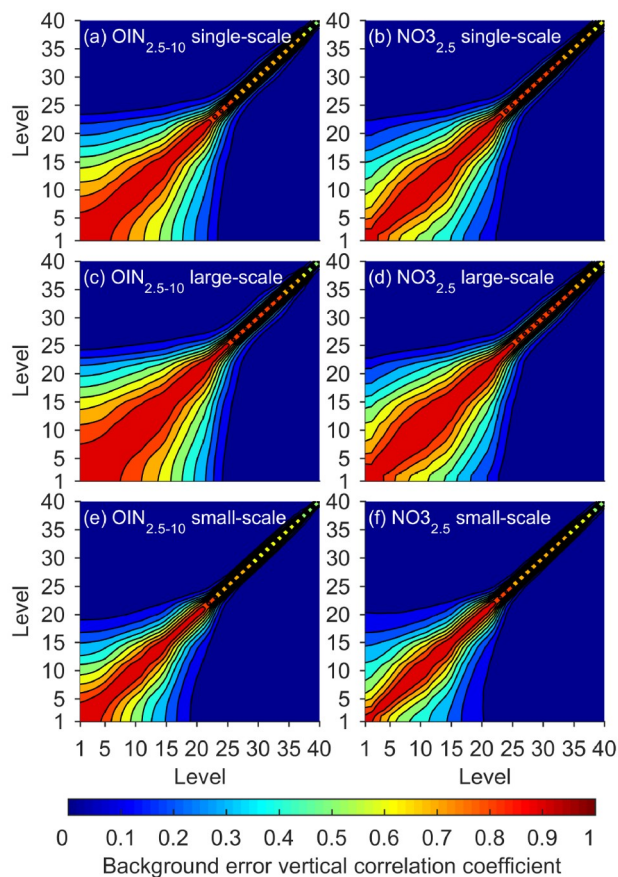
Figure 3 shows the domain-averaged BEVCC for NO3$_{2.5}$ and OIN$_{2.5-10}$ on the single-scale (BEVCC), large-scale (BEVCC$_L$), and small-scale (BEVCC$_S$). For NO3$_{2.5}$ and OIN$_{2.5-10}$, the BEVCC$_L$ was larger than BEVCC between the same two levels, whereas the BEVCC$_S$ was the smallest. The relative order of magnitude of BEVCC was similar to that of the correlation length scale, which indicates that although the Gaussian smoothing was only implemented in the horizontal direction, it had caused an adjustment in the vertical correlation of the state variables. This demonstrates that the TS-3DVAR could also spread large-scale observational information in the vertical dimension, and allow for more efficient use of small-scale information similar to that of the horizontal dimension, thereby ultimately improving the DA effect.

Table 1   Correlation length scales for the 16 state variables on the single-scale (L), large-scale (L_L) and small-scale (L_S)

State variable	EC$_{2.5}$	OC$_{2.5}$	NO3$_{2.5}$	SO4$_{2.5}$	CL$_{2.5}$	NA$_{2.5}$	NH4$_{2.5}$	OIN$_{2.5}$
L (km)	78.08	77.87	70.50	81.00	42.98	42.98	79.65	78.11
L_L (km)	116.12	116.12	109.88	118.90	98.46	98.46	117.40	115.41
L_S (km)	24.68	24.34	23.08	24.91	16.67	18.37	24.29	25.03
State variable	EC$_{2.5-10}$	OC$_{2.5-10}$	NO3$_{2.5-10}$	SO4$_{2.5-10}$	CL$_{2.5-10}$	NA$_{2.5-10}$	NH4$_{2.5-10}$	OIN$_{2.5-10}$
L (km)	68.45	69.09	53.73	67.77	25.52	25.52	59.67	50.63
L_L (km)	110.87	111.11	103.47	113.02	87.10	87.10	107.79	105.56
L_S (km)	21.07	21.15	18.90	20.58	14.92	15.90	19.13	18.44

Figure 2   Domain-averaged BESD vertical profiles for the 16 state variables on the single-scale (BESD), large-scale (BESD$_L$) and small-scale (BESD$_S$).

Figure 3 Domain-averaged BEVCC for the NO3$_{2.5}$ and OIN$_{2.5-10}$ on the single-scale (BEVCC), large-scale (BEVCC$_L$) and small-scale (BEVCC$_S$).

3.2 Effects of 3DVAR and TS-3DVAR on the PM$_{2.5}$ analyses

The DA analysis field has lesser uncertainty than the background field because the observational information is assimilated into the background field; therefore, the effect of the DA is reflected in the accuracy of aerosol analyses As shown in Figure 4a, there were higher PM$_{2.5}$ MC values in north and central China, whereas in other areas, lower values were observed. Specifically, the PM$_{2.5}$ MC at 0000 UTC 01 November 2018, was characteristically uneven overall. There were also monitoring sites whose PM$_{2.5}$ MCs were notably different from their neighboring sites, signifying a large gradient in its locality along with multiple spatial-scale characteristics of the aerosols. In relation to this, both the 3DVAR (Figure 4b) and TS-3DVAR (Figure 4c) DA fields have successfully simulated the uneven distribution pattern of the aerosols as compared with the actual observations. However, both also contained biases that were dominantly positive in most of the eastern and central China regions, based on the contour color map in Figure 4. Although both the results of the DA analyses were higher than the overall observation, the resulting difference between the TS-3DVAR and 3DVAR DA analysis fields was negative in the same

regions (Figure 4d), indicating that the TS-3DVAR DA analyses were more representative of the observations than the 3DVAR. Additionally, the analyses also had higher accuracy (Figure 5a–5c) in the small-scale characteristics. In Figure 5b, there was a large positive bias in the area of Taiyuan (TY) and Changzhi (CZ;), whereas in the TS-3DVAR bias field (Figure 5c), there were two separate large value centers in TY and CZ and with smaller bias than that in Figure 5b. In addition, there was also a large positive bias in Luoyang (LY) and Zhengzhou (ZZ; Figure 5b), but the change was in a decreasing trend due to the higher optimization of background field data on a small-scale (Figure 5c). Statistical calculations showed that the Corr and RMSE of the TS-3DVAR DA field at 0000 on November 1 were 0.889 and 13.35 μg m^{-3}, which were higher by 0.043 (5.08%) and lower by 3.78 μg m^{-3} (22.07%) than the 3DVAR DA field counterparts (Corr=0.846 and RMSE=17.13 μg m^{-3}). These results demonstrate that the TS-3DVAR generated a more accurate DA field.

Figure 6 shows the power spectra (30-day average) of the 3DVAR and TS-3DVAR DA increment fields (i.e., difference between DA analysis field and the background field) in the simulated areas. It can be observed that both the power spectra decreased with a decrease in the wavelength. In the wavelength above 405 km (15 times the grid spacing), the rate of decrease was relatively small, but the power spectra were in the order of 10^7 μg^2 m^{-6}. Contrastingly, the rate of decrease was relatively large, and the power density quickly decreased to the order of 10^3 μg^2 m^{-6} in the wavelength below 405 km, indicating the proportion of large-scale information in the DA increment fields was far greater than small-scale information, regardless of the DA method. Compared with 3DVAR, the power spectra of the TS-3DVAR DA increment field was averaged 71.70% higher than that of 3DVAR in the wavelength range of 54–216 km (2–8 times the grid spacing) and 35.33% higher at wavelengths above 351 km (13 times the grid spacing), indicating that the amplitude of the DA increment of TS-3DVAR around its mean value was greater than that of 3DVAR on these scales, and that TS-3DVAR could optimize the fluctuations of aerosols to a greater extent.

The scatter plot comparison between the PM$_{2.5}$ MC observations and PM$_{2.5}$ MCs in the 30 DA analysis fields of the 3DVAR and TS-3DVAR (Figure 7) shows that the dots from both DA analysis fields were scattered on both sides of the central line, but the dots from the TS-3DVAR (red) were closer to the central line than the 3DVAR (blue). The Corr and RMSE for the 3DVAR and the TS-3DVAR were 0.893 and 0.921, and 19.04 and 16.00 μg m^{-3}, respectively. The Corr of the latter increased by 0.03, but the RMSE decreased by 3.04 μg m^{-3}, which was 3.37% and 15.97% better than the former, indicating that the TS-3DVAR generated higher aerosol analyses accuracy, thereby improving the AQM
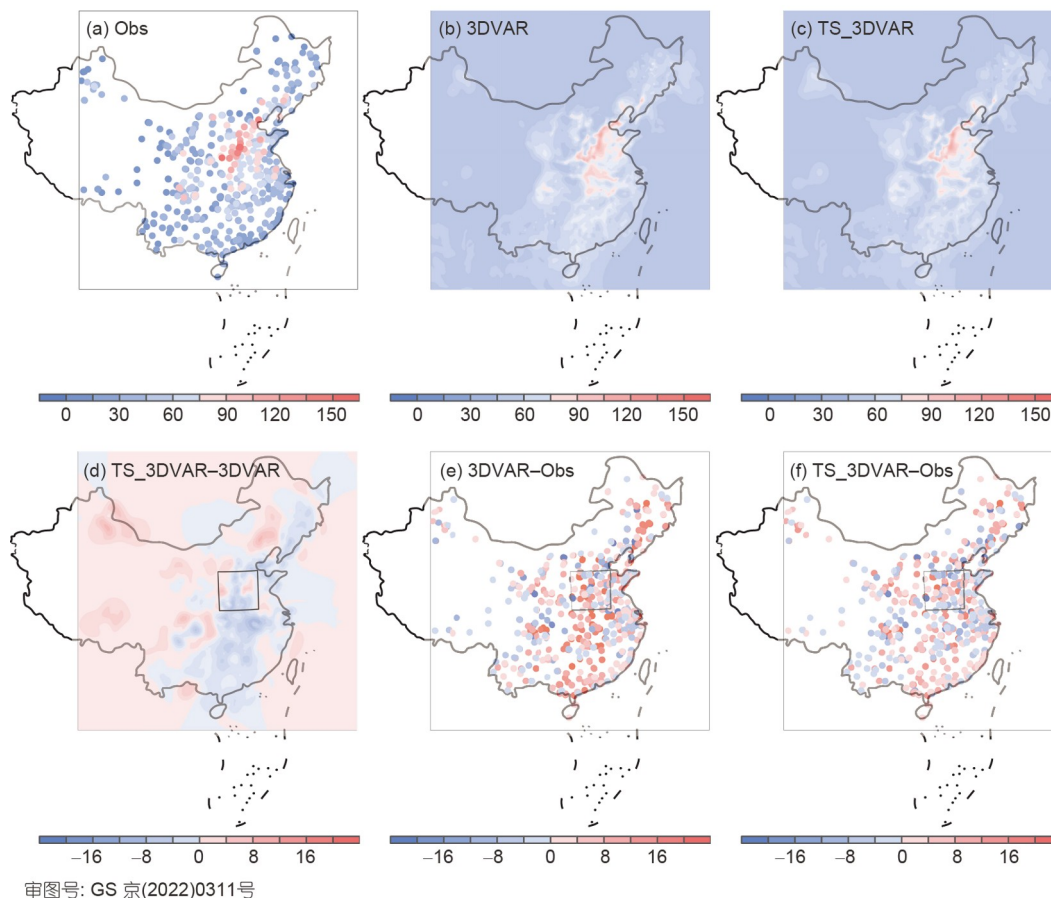
Figure 4   The PM$_{2.5}$ MC observations (a), the PM$_{2.5}$ MCs in the analysis field of 3DVAR (b) and its bias (e), in analysis field of TS-3DVAR (c) and its bias (f), the difference between the analysis of 3DVAR and TS-3DVAR (i.e., the TS-3DVAR DA analysis fields minus the 3DVAR DA analysis fields) (d) at 0000 UTC 01 November 2018.

forecasting capability for PM$_{2.5}$.

3.3   Effects of 3DVAR and TS-3DVAR on the PM$_{2.5}$ forecasting capability

It is expected that the forecasting capabilities for PM$_{2.5}$ would be improved when a more accurate DA analysis field is used as the initial chemical field of AQM. However, this improvement as well as the relative positive effects of TS-3DVAR over 3DVAR may diminish over time due to several pertinent biases such as those relating to the model and meteorological conditions, and other factors such as uncertainties of emissions. As shown in Figure 8, the 30-day Corr average of the TS-3DVAR was 0.906, which was 0.052 (6.09%) higher than that of 3DVAR (0.854), whereas the RMSE was 15.044 µg m^{-3}, or 3.446 µg m^{-3} (18.64%) lower than 3DVAR (18.490 µg m^{-3}) at the initial time. This result indicates that the initial chemical field of the TS-3DVAR was more accurate. It should be noted that the calculation method employed here was different from those that were discussed in Section 3.2, as this involved calculating the statistics each day prior to obtaining the 30-day average. The 30-day Corr

averages of both the DA were observed to fluctuate throughout the forecast—it decreased rapidly within the first 4 hours before stabilizing within 5–10 h, and by the 11th hour, it had started rapidly decreasing again. This finding may indicate that the DA could improve forecast accuracy only notably in the first 4 hours following the initial DA. During the 0–24 forecasting hours, the TS-3DVAR has a more continuous positive effect on the improvement of the forecasting ability than the 3DVAR. The 30-day Corr and RMSE averages of the TS-3DVAR within the first 4-hour were 0.637 and 30.511 µg m^{-3}. These were 0.051 (8.70%) and 3.267 µg m^{-3} (9.67%) better than that of their 3DVAR counterparts (0.586 and 33.778 µg m^{-3}). Between 5 and 10 h, the 6-hour and 30-day Corr and RMSE averages were 0.559 and 39.269 µg m^{-3}, wherein the former was 0.023 (4.29%) higher than its 3DVAR counterpart, while the latter was 2.025 µg m^{-3} (4.90%) lower. The 30-day Corr average at 0–24 h of TS-3DVAR was 0.025, which was 5.08% higher than that of 3DVAR, while the RMSE was 2.027 µg m^{-3} which was 4.85% lower. Therefore, TS-3DVAR has a relatively more positive effect on the improvement of forecasting ability, one which can potentially last over 24 h.
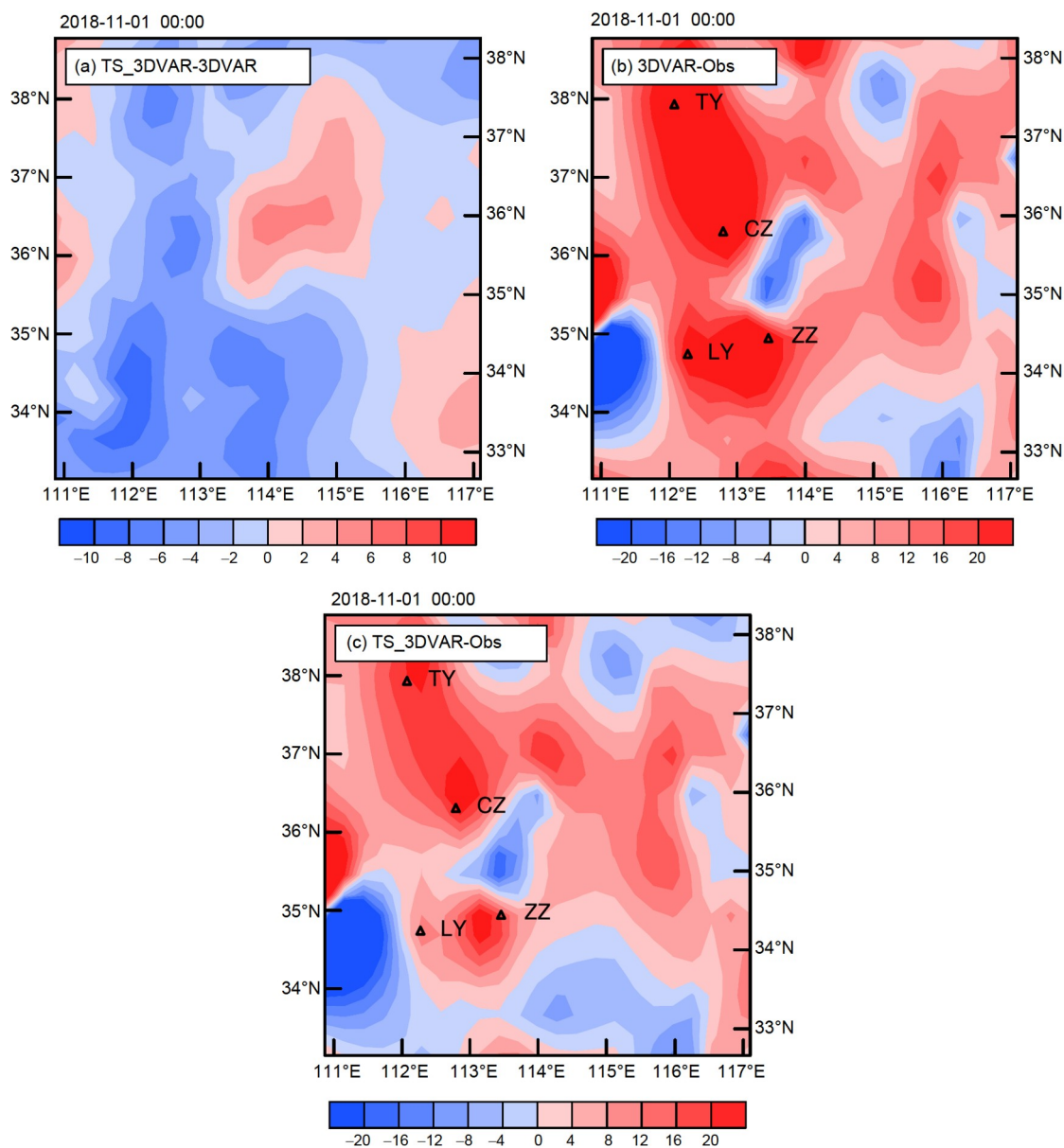
Figure 5   (a)–(c) was the sub-area of Figure 4d–4f, respectively, where Figure 5b and 5c are contour color maps derived from site values (TY: Taiyuan; CZ: Changzhi; LY: Luoyang; ZZ: Zhengzhou).

4.   Discussion and conclusion

To effectively assimilate the observations from the high-resolution aerosol observation network around the Chinese mainland and improve the aerosol forecasting capabilities of AQM, this study has extended traditional 3DVAR to a multiscale scheme with two iteration steps, named TS-3DVAR. In TS-3DVAR, the original background errors were partitioned into large-scale and small-scale using the Gaussian smoothing method, to obtain the background error standard deviation (BESD), background error vertical correlation coefficients (BEVCC), and then the horizontal correlation length scale (*L*) was estimated for both the large-scale and small-scale. The original observational innovation **d** was also

partitioned and assimilated using the background error covariance of the corresponding scale. $PM_{2.5}$ and PM_{10} observations from November 1 to November 30, 2018 were assimilated daily at 0000 UTC to determine the effects of using TS-3DVAR over 3DVAR in terms of aerosol analysis and forecast accuracy.

The average correlation length scale on large-scale and small-scale was 107.30 and 20.72 km, which were 76.71% larger and 65.88% smaller than that of the original single-scale one (60.72 km) for traditional 3DVAR. TS-3DVAR showed to have utilized more observational information on both large-scale and small-scale. The average power spectra of the TS-3DVAR assimilation increment were 71.70% and 35.33% higher than those of 3DVAR in the wavelength
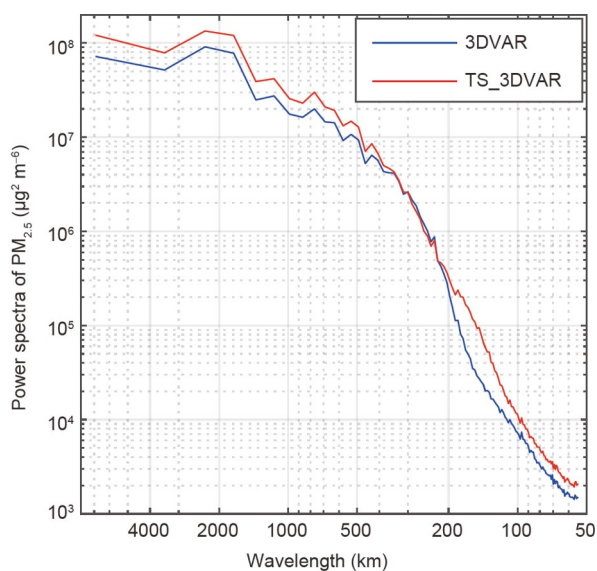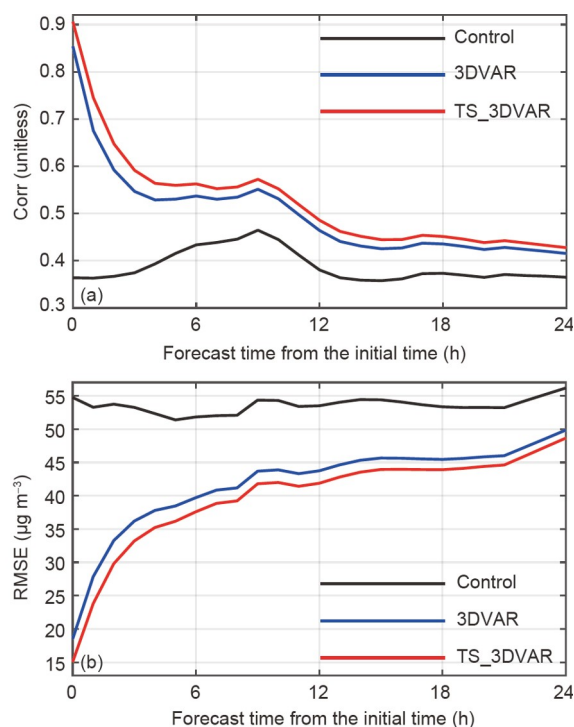
Figure 6 The power spectra (30-day average) of 3DVAR and TS-3DVAR DA increment fields (i.e., DA analysis fields minus the background field) in the simulated area.
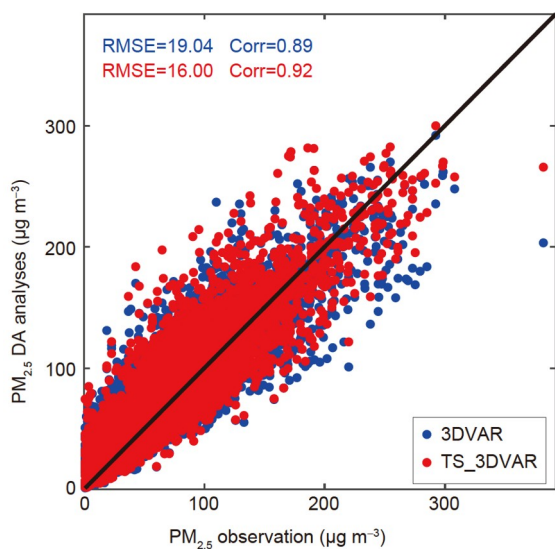
Figure 7 Scatter plot comparison between the PM$_{2.5}$ MC observations and the PM$_{2.5}$ MCs in 30 DA analysis fields of 3DVAR and TS-3DVAR.

Figure 8 Variations of the 30-day average Corr and RMSE of surface PM$_{2.5}$ MC forecasted by the Control, 3DVAR and TS-3DVAR experiments over forecast time.

ranges of 54–216 km (2–8 times the grid spacing) and those over 351 km (13 times the grid spacing). With these results, it can be concluded that TS-3DVAR had a more accurate DA analysis field by a more effective use of observational information. In the obtained initial chemical field of TS-3DVAR, the 30-day Corr of PM$_{2.5}$ was 0.052, which was 6.12% higher than that of 3DVAR. Meanwhile, the RMSE was 3.446 µg m^{-3}, or 16.4% lower. Similarly, the 30-day Corr and RMSE averages during the 0–24 hour forecast period was 0.025 and 2.027 µg m^{-3}, or 5.08% higher and 4.85% lower than its 3DVAR counterparts. Hence, the positive effects on the improvement of forecasting capability can even last for more than 24 h.

Although the results in this study showed that the TS-3DVAR can more effectively improve the accuracy of the DA analysis and subsequent forecasts for PM$_{2.5}$, enhancements may still be made on the addition of standard processes for parametric calculation and selection (i.e., horizontal correlation length scales or Gaussian smoothing), as the guidelines presented in Li et al. (2015), Muscarella et al. (2014), and Miyazawa et al. (2017) were diverse. Specifically, the optimization of these parameters was found to be associated with different factors such as the dynamic scale characteristics of assimilated observations, resolution of the observations and the model (Barker et al., 2004; Gong, 2007; Chen et al., 2015). Therefore, this aspect should be explored further. This study was limited to DA experiments for ground PM$_{2.5}$ and PM$_{10}$ observations, wherein aerosol optical thickness, extinction coefficient, or backscatter coefficient observations are not considered. Unconventional aerosol data assimilation and the simultaneous assimilation of multi-source aerosol could be different from in-situ data assimilation and be difficult as in traditional 3DVAR. As a result, there may be negative effects on the DA such as bias in the observation operator of unconventional data, redundancies and mutual interferences of multi-source data, or differences in the spatial representation of different observational data. Hence, further studies should be conducted to address these issues when using multi-scale 3DVAR. Finally, as the observation errors had been assumed in previous studies to be

uncorrelated, the correlation of observation errors in the multi-scale 3DVAR should be incorporated as the resolution of the observations increases, which may ultimately impact data assimilation.

References

Bai X P, Li H, Fang D, Costablile F, Liu F L. 2008. Application research of data assimilation in air pollution numerical prediction (in Chinese). Environ Sci, 29: 283–289

Bannister R N. 2008a. A review of forecast error covariance statistics in atmospheric variational data assimilation. I: Characteristics and measurements of forecast error covariances. Q J R Meteorol Soc, 134: 1951–1970

Bannister R N. 2008b. A review of forecast error covariance statistics in atmospheric variational data assimilation. II: Modelling the forecast error covariance statistics. Q J R Meteorol Soc, 134: 1971–1996

Bannister R N. 2017. A review of operational methods of variational and ensemble-variational data assimilation. Q J R Meteorol Soc, 143: 607–633

Barker D M, Huang W, Guo Y R, Bourgeois A J, Xiao Q N. 2004. A three dimensional variational data assimilation system for MM5: Implementation and initial results. Mon Weather Rev, 132: 897–914

Benedetti A, Morcrette J J, Boucher O, Dethof A, Engelen R J, Fisher M, Flentje H, Huneeus N, Jones L, Kaiser J W, Kinne S, Mangold A, Razinger M, Simmons A J, Suttie M. 2009. Aerosol analysis and forecast in the European Centre for medium-range weather forecasts integrated forecast system: 2. Data assimilation. J Geophys Res, 114: D13205

Bocquet M, Elbern H, Eskes H, Hirtl M, Zabkar R, Carmichael G R, Flemming J, Inness A, Pagowski M, Perez Camano J L, Saide P E, San Jose R, Sofiev M, Vira J, Baklanov A, Carnevale C, Grell G, Seigneur C. 2015. Data assimilation in atmospheric chemistry models: Current status and future prospects for coupled chemistry meteorology models. Atmos Chem Phys, 15: 5325–5358

Boylan J W, Russell A G. 2006. PM and light extinction model performance metrics, goals, and criteria for three-dimensional air quality models. Atmos Environ, 40: 4946–4959

Cao X Q, Huang S X, Zhang W M, Du H D. 2008. Modeling background error covariance in regional 3D-VAR (in Chinese). J Meteorol Sci Sci Meteorol Sin 28: 8–14

Chen D, Liu Z, Ban J, Chen M. 2019. The 2015 and 2016 wintertime air pollution in China: SO$_2$ emission changes derived from a WRF-Chem/EnKF coupled data assimilation system. Atmos Chem Phys, 19: 8619–8650

Chen P L, Wang T J, Dong M, Kasoar M, Han Y, Xie M, Li S, Zhuang B L, Li M M, Huang T N. 2017. Characterization of major natural and anthropogenic source profiles for size-fractionated PM in Yangtze River Delta. Sci Total Environ, 598: 135–145

Chen S Y, Huang J P, Qian Y, Zhao C, Kang L T, Yang B, Wang Y, Liu Y Z, Yuan T G, Wang T H, Ma X J, Zhang G L. 2017. An overview of mineral dust modeling over East Asia. J Meteorol Res, 31: 633–653

Chen Y D, Xia X, Min J Z, Huang X Y, Rizvi S R H. 2016. Balance characteristics of multivariate background error covariance for rainy and dry seasons and their impact on precipitation forecasts of two rainfall events. Meteorol Atmos Phys, 128: 579–600

Chen Y D, Zhao X, Min J Z, Fan S Y, Wang Y B, Zeng L M. 2015. Comparative analysis of characteristics for background error covariances in Tibetan Plateau and East China (in Chinese). Trans Atmos Sci, 38: 650–657

Cheng X H, Liu Y L, Xu X D, You W, Zang Z L, Gao L N, Chen Y B, Su D B, Yan P. 2019. Lidar data assimilation method based on CRTM and WRF-Chem models and its application in PM$_{2.5}$ forecasts in Beijing. Sci Total Environ, 682: 541–552

Dai T, Schutgens N A J, Goto D, Shi G Y, Nakajima T. 2014. Improvement of aerosol optical properties modeling over Eastern Asia with MODIS AOD assimilation in a global non-hydrostatic icosaheral aerosol transport model. Environ Pollut, 195: 319–329

Feng S Z, Jiang F, Wang H M, Wang H K, Ju W M, Shen Y, Zheng Y H, Wu Z, Ding A J. 2020. NO$_x$ emission changes over China during the COVID-19 epidemic inferred from surface NO$_2$ observations. Geophys Res Lett, 47: e90080

Gong J D. 2007. The analysis on variation of horizontal de-correlation length with model resolution in data assimilation system (in Chinese). Chin J Atmos Sci, 31: 459–467

Ha J H, Lee D K. 2012. Effect of length scale tuning of background error in WRF-3DVAR system on assimilation of high-resolution surface data for heavy rainfall simulation. Adv Atmos Sci, 29: 1142–1158

Han X, Zhang M. 2021. The interannual variation of transboundary contributions from Chinese emissions of PM$_{2.5}$ to South Korea. Adv Atmos Sci, 38: 701–706

Hu Y W, Zang Z L, Chen D, Ma X Y, Liang Y F, You W, Pan X B, Wang L Q, Wang D C, Zhang Z D. 2022. Optimization and evaluation of SO$_2$ emissions based on WRF-Chem and 3DVAR data assimilation. Remote Sens, 14: 220

Huang Q, Wang T J, Chen P L, Huang X X, Zhu J L, Zhuang B L. 2017. Impacts of emission reduction and meteorological conditions on air quality improvement during the 2014 Youth Olympic Games in Nanjing, China. Atmos Chem Phys, 17: 13457–13471

Ide K, Courtier P, Ghil M, Lorenc A C. 1997. Unified notation for data assimilation: Operational, sequential and variational. J Meteorol Soc Jpn, 75: 181–189

Jiang Z Q, Liu Z Q, Wang T J, Schwartz C S, Lin H C, Jiang F. 2013. Probing into the impact of 3DVAR assimilation of surface PM$_{10}$ observations over China using process analysis. J Geophys Res-Atmos, 118: 6738–6749

Li Z J, Chao Y, McWilliams J C, Ide K. 2008. A three-dimensional variational data assimilation scheme for the Regional Ocean Modeling System. J Atmos Ocean Tech, 25: 2074–2090

Li Z J, Cheng X P, Gustafson W I, Vogelmann A M. 2016. Spectral characteristics of background error covariance and multiscale data assimilation. Int J Numer Meth Fluids, 82: 1035–1048

Li Z J, McWilliams J C, Ide K, Farrara J D. 2015. A multiscale variational data assimilation scheme: Formulation and Illustration. Mon Weather Rev, 143: 3804–3822

Li Z J, Zang Z L, Li Q B, Chao Y, Chen D, Ye Z, Liu Y, Liou K N. 2013. A three-dimensional variational data assimilation system for multiple aerosol species with WRF/Chem and an application to PM$_{2.5}$ prediction. Atmos Chem Phys, 13: 4265–4278

Liang Y F, Zang Z L, Liu D, Yan P, Hu Y, Zhou Y, You W. 2020. Development of a three-dimensional variational assimilation system for lidar profile data based on a size-resolved aerosol model in WRF-Chem model v3.9.1 and its application in PM$_{2.5}$ forecasts across China. Geosci Model Dev, 13: 6285–6301

Liu Z J, Wang T J, Xie M, Li S, Zhuang B L, Han Y. 2015. Influence of winter monsoon on aerosol transport and distribution in East Asia (in Chinese). J Nanjing Univ Nat Sci, 51: 575–586

Liu Z Q, Liu Q H, Lin H C, Schwartz C S, Lee Y H, Wang T J. 2011. Three-dimensional variational assimilation of MODIS aerosol optical depth: Implementation and application to a dust storm over East Asia. J Geophys Res, 116: D23206

Miyazawa Y, Varlamov S M, Miyama T, Guo X, Hihara T, Kiyomatsu K, Kachi M, Kurihara Y, Murakami H. 2017. Assimilation of high-re-

solution sea surface temperature data into an operational nowcast/forecast system around japan using a multi-scale three-dimensional variational scheme. Ocean Dyn, 67: 713–728

Muscarella P A, Carrier M J, Ngodock H E. 2014. An examination of a multi-scale three-dimensional variational data assimilation scheme in the Kuroshio Extension using the naval coastal ocean model. Cont Shelf Res, 73: 41–48

Niu T, Gong S L, Zhu G F, Liu H L, Hu X Q, Zhou C H, Wang Y Q. 2008. Data assimilation of dust aerosol observations for the CUACE/dust forecasting system. Atmos Chem Phys, 8: 3473–3482

Pagowski M, Grell G A. 2012. Experiments with the assimilation of fine aerosols using an ensemble Kalman filter. J Geophys Res, 117: D21302

Pang J M, Wang X M. 2021. The impacts of background error covariance on particulate matter assimilation and forecast: An ideal case study with a modal aerosol model over China. Sci Total Environ, 786: 147417

Parrish D F, Derber J C. 1992. The National Meteorological Center's spectral statistical-interpolation analysis system. Mon Weather Rev, 120: 1747–1763

Peng S Q, Xie L, Liu B, Semazzi F. 2010. Application of scale-selective data assimilation to regional climate modeling and prediction. Mon Weather Rev, 138: 1307–1318

Peng Z, Liu Z, Chen D, Ban J. 2017. Improving $PM_{2.5}$ forecast over China by the joint adjustment of initial conditions and source emissions with an ensemble Kalman filter. Atmos Chem Phys, 17: 4837–4855

Sandu A, Chai T. 2011. Chemical data assimilation—An overview. Atmosphere, 2: 426–463

Sun W, Liu Z, Chen D, Zhao P, Chen M. 2020. Development and application of the WRFDA-Chem three-dimensional variational (3DVAR) system: Aiming to improve air quality forecasting and diagnose model deficiencies. Atmos Chem Phys, 20: 9311–9329

Tang X, Zhu J, Wang Z F, Gbaguidi A, Lin C Y, Xin J Y, Song T, Hu B. 2016. Limitations of ozone data assimilation with adjustment of NO_x emissions: Mixed effects on NO_2 forecasts over Beijing and surrounding areas. Atmos Chem Phys, 16: 6395–6405

Wang D, You W, Zang Z, Pan X, He H, Liang Y. 2020. A three-dimensional variational data assimilation system for a size-resolved aerosol model: Implementation and application for particulate matter and gaseous pollutant forecasts across China. Sci China Earth Sci, 63: 1366–1380

Wang D C, You W, Zang Z L, Pan X B, Hu Y W, Liang Y F. 2022. A three-dimensional variational data assimilation system for aerosol optical properties based on WRF-Chem v4.0: Design, development, and application of assimilating Himawari-8 aerosol observations. Geosci Model Dev, 15: 1821–1840

Wang P Q, Li Y N, Peng S Q. 2016. Application of scale-selective data assimilation method in ocean modeling: simulation of a strong warm eddy in Xisha (in Chinese). J Trop Oceanogr, 35: 30–39

Xia X L, Min J Z, Shen F F, Wang Y B, Yang C. 2019. Aerosol data assimilation using data from Fengyun-3A and MODIS: Application to a dust storm over East Asia in 2011. Adv Atmos Sci, 36: 1–14

Xie Y, Koch S, McGinley J, Albers S, Bieringer P E, Wolfson M, Chan M. 2011. A space-time multiscale analysis system: A sequential variational analysis approach. Mon Weather Rev, 139: 1224–1240

Xu X D, Zhou X J, Shi X H. 2005. The spatial structure and scale characteristics of the effects of the air pollution sources in urban communities (in Chinese). Sci China Ser D-Earth Sci, 35(Suppl I): 1–19

Yin X M, Dai T, Schutgens N A J, Goto D, Nakajima T, Shi G Y. 2016. Effects of data assimilation on the global aerosol key optical properties simulations. Atmos Res, 178-179: 175–186

Zang Z L, Hao Z L, Pan X B, Li Z J, Chen D, Zhang L, Li Q B. 2015. Background error statistics for aerosol variables from WRF/chem predictions in Southern California. Asia-Pac J Atmos Sci, 51: 103–114

Zang Z L, Li Z J, Pan X B, Hao Z L, You W. 2016. Aerosol data assimilation and forecasting experiments using aircraft and surface observations during CalNex. Tellus B-Chem Phys Meteorol, 68: 29812

Zaveri R A, Easter R C, Fast J D, Peters L K. 2008. Model for simulating aerosol interactions and chemistry (MOSAIC). J Geophys Res, 113: D13204

Zhang M G. 2005. A multi-scale air quality modeling system and its evaluation I. Introduction to the model system and simulation of meteorological parameters (in Chinese). Chin J Atmos Sci, 29: 805–813

Zhang X B, Tan Z M. 2013. On the optimal background error covariances: Different scale errors' contribution. J Trop Meteor, 19: 305–321

Zhang X B, Xue J S, Wan Q L, Ding W Y, Li H R. 2014. Study on time-dependent and multi-scale background error covariance I——Construction (in Chinese). J Trop Meteorol, 30: 675–686

Zhang X B, Xue J S, Wan Q L, Ding W Y, Li H R. 2015. Study on time-dependent and multi-scale background error covariance II——Application (in Chinese). J Trop Meteorol, 31: 161–172

Zhu B, Wang H L, Shen L J, Kang H Q, Yu X N. 2013. Aerosol spectra and new particle formation observed in various seasons in Nanjing. Adv Atmos Sci, 30: 1632–1644

Zhu J, Tang X, Wang Z F, Wu L. 2018. A review of air quality data assimilation methods and their application (in Chinese). Chin J Atmos Sci, 42:607–620

(Responsible editor: Lili LEI)